CHEMISTRY OF MATERIALS

Subscriber access provided by UNIV OF PITTSBURGH

Article

Phase Stability, Crystal Structure, and Thermoelectric Properties of Cu12Sb4S13-xSex Solid Solutions

Xu Lu, Donald T. Morelli, Yuxing Wang, Wei Lai, Yi Xia, and Vidvuds Ozolins

Chem. Mater., **Just Accepted Manuscript** • DOI: 10.1021/acs.chemmater.5b04796 • Publication Date (Web): 19 Feb 2016

Downloaded from http://pubs.acs.org on February 21, 2016

Just Accepted

"Just Accepted" manuscripts have been peer-reviewed and accepted for publication. They are posted online prior to technical editing, formatting for publication and author proofing. The American Chemical Society provides "Just Accepted" as a free service to the research community to expedite the dissemination of scientific material as soon as possible after acceptance. "Just Accepted" manuscripts appear in full in PDF format accompanied by an HTML abstract. "Just Accepted" manuscripts have been fully peer reviewed, but should not be considered the official version of record. They are accessible to all readers and citable by the Digital Object Identifier (DOI®). "Just Accepted" is an optional service offered to authors. Therefore, the "Just Accepted" Web site may not include all articles that will be published in the journal. After a manuscript is technically edited and formatted, it will be removed from the "Just Accepted" Web site and published as an ASAP article. Note that technical editing may introduce minor changes to the manuscript text and/or graphics which could affect content, and all legal disclaimers and ethical guidelines that apply to the journal pertain. ACS cannot be held responsible for errors or consequences arising from the use of information contained in these "Just Accepted" manuscripts.

ACS Publications

Chemistry of Materials is published by the American Chemical Society. 1155 Sixteenth Street N.W., Washington, DC 20036

Published by American Chemical Society. Copyright © American Chemical Society. However, no copyright claim is made to original U.S. Government works, or works produced by employees of any Commonwealth realm Crown government in the course of their duties.

Phase Stability, Crystal Structure, and Thermoelectric Properties of $Cu_{12}Sb_4S_{13-x}Se_x$ Solid Solutions

Xu Lu[1,2]*, Donald T. Morelli[2]*, Yuxing Wang[2], Wei Lai[2], Yi Xia[3]and Vidvuds Ozolins[3]

[1]College of Physics, Chongqing University, Chongqing 401331, People's Republic of China

[2]Department of Chemical Engineering & Materials Science, Michigan State University, East Lansing, Michigan 48824 USA

[3]Department of Materials Science & Engineering, University of California-Los Angeles, Los Angeles, California 90095 USA

ABSTRACT: The solubility of selenium on the sulfur site in tetrahedrite $Cu_{12}Sb_4S_{13}$ has been investigated by theoretical calculations, and the results have been verified by x-ray diffractionand x-ray synchrotron studies on $Cu_{12}Sb_4S_{13-x}Se_x$ with x ranging from zero to 3. Density-functional theory calculations predict that Se substitution on the tetrahedral 24g site is preferred, and this is found to be consistent with Rietveld refinement of the crystal structure. Hightemperature thermoelectric property measurements on $Cu_{12}Sb_4S_{13-x}Se_x$ reveal that Se substitution results in a decrease in electrical resistivity without diminution of the Seebeck coefficient. The "decoupling" of these parameters leads to a 30% enhancement in power factor of the x = 1 sample compared to that of pure $Cu_{12}Sb_4S_{13}$.In addition, in spite of an increased electronic thermal conductivity, alloy scattering of phonons caused by Se substitution reduces both thelattice and total thermal conductivities, leading to a large increase in the thermoelectric figure of merit.

INTRODUCTION

The increasing demand in world's energy consumption and emergent requirement for reduction in greenhouse gases emission motivate the research in thermoelectric materials and relevant devices[1]. For large scale application in waste heat recovery in industry, the promising thermoelectric materials should contain low cost, earth abundant and nontoxic elements[2]. Natural mineral tetrahedrite-based compounds $Cu_{12-x}M_xSb_4S_{13}$, in which M are transition metals like Zn, Fe, Ni, Co and Mn, were recently reported to be among the best performing p-type thermoelectric (TE) materials[2-10]. The dimensionless figure of merit, defined as $zT = S^2/\rho k$, where S,ρ, and k are the Seebeck coefficient, electrical resistivity and total thermal conductivity, respectively, is used to evaluate the performance of TE materials. While pure synthetic tetrahedrite $Cu_{12}Sb_4S_{13}$ has a zT value of approximately 0.6 at 700 K, the values of transition metal substituted tetrahedrite compounds are in the range of 0.7-1.1. These enhancements in the figure of merit occur through a reduction in thermal conductivity; in all cases, the power factor, (S^2/ρ), over the M-substituted samples is reduced relative to pure tetrahedrite.

While there have been several studies of the thermoelectric properties of compounds synthesized using substitutions for copper and antimony[11,12] in tetrahedrite, experimental investigations of anion site substitution have not yet been reported. The $Cu_{12}Sb_4Se_{13}$ phase was recently predicted by Zhang, et al[13]. to be stable at high temperatures and isostructural with $Cu_{12}Sb_4S_{13}$. Electronic structure and phonon calculations indicated that $Cu_{12}Sb_4Se_{13}$ could be a promising TE material with low thermal conductivity. Our previous attempts to synthesize this compound, however, were

unsuccessful, leading us to investigate the possibility of synthesizing $Cu_{12}Sb_4S_{13-x}Se_x$ solid solutions from the end member of pure tetrahedrite $Cu_{12}Sb_4S_{13}$. Here we report the successful synthesis of these solid solutions and further demonstrate that the power factor of $Cu_{12}Sb_4S_{13}$ can be increased by Se substitution for S. In the traditional carrier concentration adjustment approach for power factor enhancement, the Seebeck coefficient decreases with reduced electrical resistivity. In contrast, the Seebeck coefficient of $Cu_{12}Sb_4S_{13-x}Se_x$ solid solutions remains unchanged with decreasing electrical resistivity. This unusual "decoupling" of these parameters is due to an increase in band degeneracy with selenium substitution, and leads directly to an increase in thermoelectric performance.

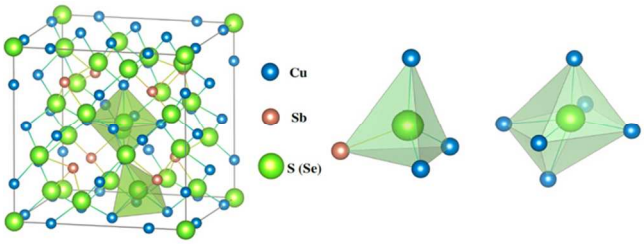

Figure 1. The tetrahedrite crystal structure (left) and two bonding of the selenium atom substituting for sulfur after full relaxation at the tetrahedral 24g (middle) and octahedral 2a (right) sites respectively.

COMPUTATIONALAND EXPERIMENTAL SECTION

Materials Structural stability and phase diagram calculations. Structural relaxation and accurate free energy calculations were performed using the projector-augmented wave (PAW) method which is implemented in the highly efficient Vienna Ab-initio Simulation Package (VASP)[14-17]. Perdew-Becke-Ernzerhof (PBE)[18,19] generalized gradient approximation (GGA) for the exchange-correlation functional and plane wave basis with the cutoff energy of 450 eV were used in all calculations. Structures of competing phases – Cu, $Cu_{12}Sb_4S_{13}$, Cu_3SbS_4, Cu_3SbSe_4, Cu_3Se_2, Cu_7S_4, CuS, $CuSbS_2$, $CuSbSe_2$, CuSe, $CuSe_2$, S, Sb, Sb_2S_3, Sb_2Se_3 and Se – were fully relaxed until all forces were below 0.02 eV/Å. The total energies of pure and Se-substituted tetrahedrites were calculated on regularly spaced k-point meshes consistent with a given constant k-point density corresponding to 10×10×10 for the tetrahedrite primitive cell. Pure tetrahedrite is dynamically unstable at T=0 K under cubic symmetry, preferring to distort into a rhombohedral R3 structure with an energy lowering of approximately 65 meV per formula unit. We used the energy of the rhombohedral structure as reference for calculating Se substitution energies. Energy-preferred Se sites were identified by choosing the lowest energy state among all the symmetry-inequivalent configurations for 1 and 2 Se atoms within the rhombohedral unit cell. Formation energy of $Cu_{12}Sb_4S_{10}Se_3$ was obtained by fixing 2 Se atoms to the lowest-energy configuration for $Cu_{12}Sb_4S_{11}Se_2$ and enumerating all symmetrically inequivalent possibilities for substituting the third Se.

The stability of Se-doped tetrahedrite is characterized by its formation energy, which is determined by a constrained linear optimization procedure as follows[20]. In the Cu-Sb-S-Se quaternary phase diagram, we include all known elemental, binary, and ternary phases and we detect which combination of phase forms the T-0 K equilibrium tetrahedron which contains the $Cu_{12}Sb_4S_{13-x}Se_x$. This is achieved by minimizing the total energy over all multiphase mixtures of competing compounds with the same overall composition as Se-substituted tetrahedrite:

$$E_0 = \min_{\{f_p\}} \sum_p f_p E_p \quad \text{s.t.} \quad \sum_p f_p n_{ip} = y_i, \qquad (1)$$

where fp is the number of moles of phase p, Ep is the molar energy of p, nip is the number of atoms of type i per formula unit of phase p, and yi represent the composition of $Cu_{12}Sb_4S_{13-x}Se_x$ (yCu=12, ySb=4, yS=13-x, and ySe=x). The formation energy of $Cu_{12}Sb_4S_{13-x}Se_x$ is defined as

$$\Delta E(x) = E(Cu_{12}Sb_4S_{13-x}Se_x) - E_0(x) \qquad (2)$$

Sample synthesis, crystal structure, and thermoelectric property measurement. Samples were prepared by vacuum melting, long-term heat treatment, and hot pressing as described in our previous studies[2-4], in which the starting elements- Cu(99.99 %, Alfa-Aesar), Sb(99.9999 %, Alfa-Aesar), and S , Se (99.999%, Alfa-Aesar) were used. Crystal structure was investigated by both lab powder x-ray diffraction (XRD) and high-resolution X-ray synchrotron (HRXRS) studies. Powdered samples were scanned in a RigakuMiniflex II x-ray diffractometer over a 2θ range of 20 – 90 degrees using CuKα radiation. The high-resolution X-ray synchrotron powder diffraction data from 10 to 180 degrees were collected at the 11BM beamline at Advanced Photon Source (APS) at 295 K using a wavelength of 0.459004 Å. Rietveld refinement was carried out using the software package Jana2006[21].

Electrical resistivity and Seebeck coefficient were measured over the temperature range of 300-750 K using an Ulvac ZEM-3 system. Total thermal conductivity was calculated from the product of thermal diffusivity (Netzsch LFA-457), specific heat (Netzsh DSC 200 F3 Maia) and density (Archimedes method). The errors in our electrical and thermal transport measurement are estimated to be 5% and 10%, respectively.

RESULTS AND DISCUSSION

Structural stability and phase diagram calculations. There are two distinct S sites in cubic tetrahedrite, indicated as S(1) and S(2), which are shown in Figure 1. The S(1) atoms (24g site) are tetrahedrally coordinated by two Cu(12d site), one Cu(12e site), and Sb(8c site), while

S(2) is surrounded by six Cu atoms in a regular octahedral coordination (2a site)[22]. We considered Se substitution for S on both types of sites. Se substitution on the tetrahedral 24g sites is energetically preferred over the octahedral 2a site by approximately 43 meV/Se. We find that all Se-substituted tetrahedrite phases lie within the composition space tetrahedron composed of Cu, $Cu_{12}Sb_4S_{13}$, Cu_3Se_2 and $CuSbSe_2$ (Figure 2 (a)), which are the relevant competing phases in Eq. (1). The formation energy of Se substitution as a function of the number of Se atoms is displayed in Figure 2 (b). Substituting one Se atom per unit cell has a small positive formation energy of approximately 20 meV per formula unit, while additional substitution of a second Se atom increases the formation energy to slightly above 30 meV per formula unit. Substitution of the third Se is energetically neutral leaving the total formation energy per formula unit unchanged. These formation energy values are small in comparison with the free energy of mixing, which can be roughly approximated by $\Delta F_{\mathrm{mix}} = 12k_BT[x'\ln x' + (1-x')\ln(1-x')]$, where the factor 12 accounts for 12 tetrahedral S(1) sites in the unit cell, and $x' = x/12$. Therefore, static total energy calculations predict complete miscibility for Se on the S(1) sites in tetrahedrite at room temperature and above. We note that our calculations do not take into account effects of vibrational entropy, which were found to play a significant role in the phase stability of compounds in the Cu-Sb-Se system[23] Calculated static total energies suggest that more than Se = 2 atoms/unit cell can be substituted on the S sites. However, accounting vibrational entropy could change the predicted solubility limit because the formation free energies are fairly small; unfortunately, vibrational entropies are very difficult to calculate for these compounds due to the highly anharmonic nature of atomic vibrations, such as existence of harmonically unstable optical modes. Furthermore, existence of a previously unknown quaternary phase is possible and it would lower the solubility limit.

Experimental crystal structure. Figure. 2 (c) shows the (XRD) patterns for $Cu_{12}Sb_4S_{13-x}Se_x$ (x = 0.5, 1, 2, 3). No second phases are detected up to x = 2. A peak shift to the lower angle is observed, indicating an expansion of the unit cell upon substitution of the larger Se ion. For x = 3, two tiny additional peaks appear near the strongest peak as indicated by arrow, and these remain even after two weeks of heat treatment, indicating an excess substitution of Se over solubility limit. The calculated lattice constants of all samples from Rietveld analyses are provided in support information (Figure S1). The lattice constants increase with increasing Se content due to larger ionic radius of Se atoms, showing only small deviation from expected linear curve. It can be concluded that most of Se atoms successfully substitute S atoms in those compounds even though there could be still tiny portion of second phase.

The samples with x = 0 and x = 1 were studied in more detail using x-ray synchrotron radiation and Rietveld refinement. For the x = 0 sample, strong anisotropic atomic displacement was found for the Cu-12e site (U11 = 0.0846 Å2, U22 = U11, U33 = 0.0225 Å2, U12 = -0.0582 Å2, U13 = U23 = 0)[24]. These values are similar to those reported earlier for the same compounds[23]. Such anisotropic atomic displacement parameters (ADPs) indicate strong out-of-plane vibration of the Cu-12e site, consistent with that reported for the same compound and Ni-doped sample[6]. For the x = 1 sample, if Se atoms are placed both at the 2a and 24g sites, Rietveld refinement yielded the occupancy of Se at the 2a site close to zero. This suggests that Se atoms are incorporated into the 24g sites, which is in agreement with our DFT-based formation energy calculations. Furthermore, stronger out-of-plane vibration was found for the Cu-12e site in the x = 1 sample, from examination of ADPs (U11 = 0.0925 Å2, U22 = U11, U33 = 0.021 Å2, U12 = -0.0648 Å2, U13 = U23 = 0, Table S1). We hypothesize that the larger ADPs contribute to lowering the lattice thermal conductivity of the x = 1 sample, as will be discussed in the following section.

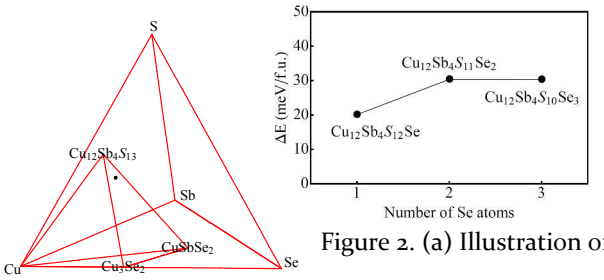

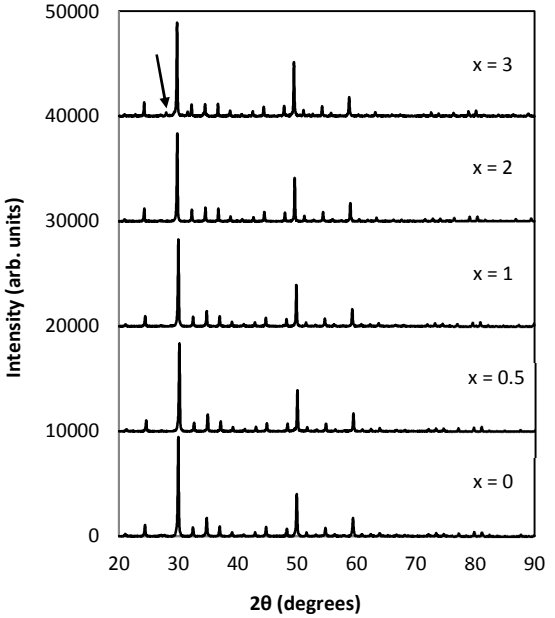

Figure 2. (a) Illustration of quaternary phase diagram and the equilibrium tetrahedron in which Se-doped tetrahedrite lies (upper left); (b) Formation energy per primitive cell as a function of the number of Se atoms in Se substituted tetrahedrite (upper right); (c) XRD patterns of $Cu_{12}Sb_4S_{13-x}Se_x$ (x = 0, 0.5, 1, 2, 3, bottom to top) (lower).

A recent study reported that an exsolution process occurs at 250 K and 373 K for $Cu_{12}Sb_{4-x}Te_xS_{13}$ and $Cu_{12}Sb_4S_{13}$, respectively[25], showing a strong peak splitting due to phase seperation. Our lab XRD patterns of $Cu_{12}SbS_{12}Se$ (Figure S2c) show no signs of similar peak splitting observed in the reference while the small shoulders in the synchrotron patterns (Figure S2a) indicated the possibility of phase separation. The Rietveld refinement of a two-phase model (Figure S2b) suggests a mixing of $Cu_{12}SbS_{12}Se$ (93.03 vol%) and $Cu_{12}SbS_{13}$ (6.97 vol%) phases (Table S2). The effect of two phases on thermoelectric transport will be discussed in the next section.

Thermoelectric Properties. The electrical transport properties of $Cu_{12}Sb_4S_{13-x}Se_x$ (x = 0, 0.5, 1, 2) are shown in Figure. 3. The resistivity of all samples has the same temperature dependent character, first decreasing with temperature from room temperature to 400 K, and then flattening. At high temperatures (600 to 720 K), the resistivity increases with increasing temperature; in this range, all the carriers have been activated, and carrier-phonon scattering begins to dominate, leading to a decreased mobility and thus increased resistivity, which was observed in other synthetic tetrahedrites[2,10,11]. For all the Se substituted samples, the resistivity is reduced over the entire temperature range compared to that of the pure sample. However, the Seebeck coefficients of the Se substituted samples do not decrease. Inherently, the Seebeck coefficient and electrical resistivity are both related to carrier concentration, exhibiting a coupled relationship in most materials. Electronic structure calculations show that the substitution of one Se atom in the tetrahedrite unit cell moves an additional valence band close to the Fermi level, providing an additional pathway for charge carrier transport without altering the Seebeck coefficient[26]. Considering two bands are responsible for electronic transport, the total Seebeck coefficient would be a weighted average of the Seebeck coefficients of each band. In most of the cases, the band with the higher conductivity, which typically has more carriers and thus smaller Seebeck coefficient, is more strongly weighted, leading to a decrease in total Seebeck coefficient. However, when the energies of two are close to each other or saying degenerate, if the two bands have the same Seebeck coefficient, the total Seebeck coefficient can be maintained while the total electrical resistivity is substantially lower than that of either band alone. The similar mechanism involving increased band degeneracy has recently been reported in $PbTe_{1-x}Se_x$[27] and $Mg_2Si_{1-x}Sn_x$[28] solid solutions. For the x = 2 sample, an increase in electrical resistivity is observed. The electronic transport taking place among multiple bands may cause strong inter-valley scattering, reducing the mobility of charge carriers. However, it is also possible, in light of the rapid increase in formation energy for the second Se substitution shown in Figure 2 (b), that there are unsuccessfully substituting Se atoms existing in interstitial sites of x = 2 sample, serving as scattering centers for carrier transport. The combination of reduced electrical resistivity with unchanged Seebeck coefficient caused by Se substitution leads to the improvement in power factor of tetrahedrite. The power factor reaches a maximum value of 16 μW/cm K² for the x = 1 sample, a 30% enhancement relative to that of the x = 0 sample. It should be noted that the synchrotron XRD patterns show the separation of $Cu_{12}Sb_4S_{12Se}$ and $Cu_{12}Sb_4S_{13}$ phases. Considering the small portion of $Cu_{12}Sb_4S_{13}$ (less than 7 %) in the mixture and smaller power factor of $Cu_{12}Sb_4S_{13}$, the enhanced power factor should result from the intrinsic transport properties of $Cu_{12}Sb_4S_{12-x}Se_x$ solid solutions rather than the effect of phase separation.

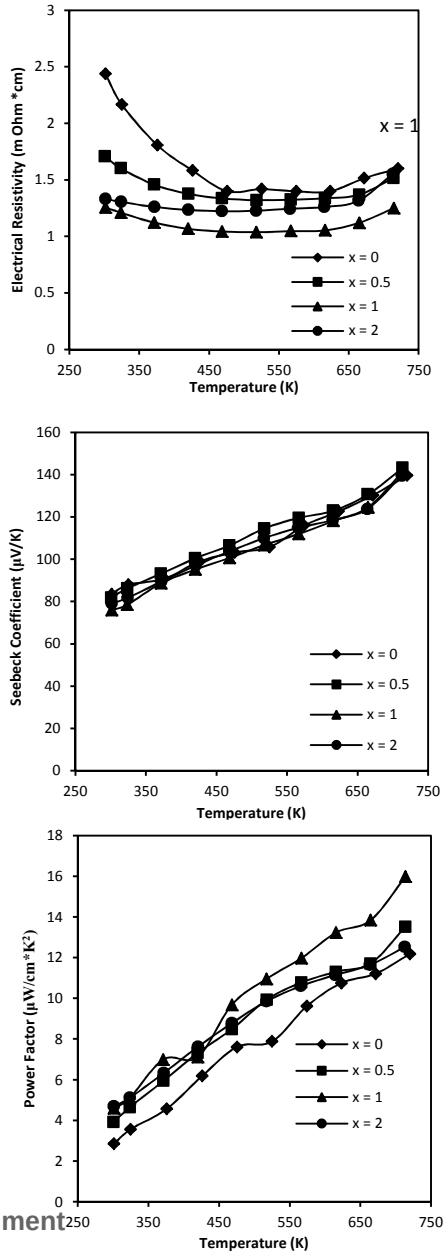

Figure 3. Temperature dependence of the electrical transport properties of $Cu_{12}Sb_4S_{13-x}Se_x$ (x = 0, 0.5, 1, 2). While the electrical resistivity (upper) decreases as Se is added, the Seebeck coefficient (center) remains unchanged, resulting in enhancement of the thermoelectric power factor (lower).

The total thermal conductivity is shown in Figure 4 (upper). Again, the samples all display a similar temperature dependence: the thermal conductivity increases from room temperature to 600 K, then begins to fall. This diminution is consistent with a decrease in the electronic contribution of thermal conductivity due to the increasing electrical resistivity shown in Figure 3. Although pure $Cu_{12}Sb_4S_{13}$ has the highest electrical resistivity and thus smallest electronic contribution to total thermal conductivity, all the Se substituted samples have lower total thermal conductivity over the entire temperature range. This implies a large reduction in the lattice thermal conductivity in Se substituted samples. To clarify this, we subtract the electronic thermal conductivity from the total thermal conductivity to estimate the lattice thermal conductivity of $Cu_{12}Sb_4S_{13-x}Se_x$ (x = 0, 0.5, 1). Since x = 2 sample may have interstitial Se or small amount of other second phases which is implied by electrical resistivity and theoretical formation energy calculation but not shown in XRD patterns, the calculated lattice thermal conductivity is not included here. The electronic thermal conductivity is approximated by the Wiedemann-Franz law $\kappa_e = LT/\rho$, where T is the absolute temperature. The Lorenz numbers L are calculated using[29]

$$L = \frac{k_B^2}{e^2}\frac{3F_0(\eta)F_2(\eta) - 4F_1^2(\eta)}{F_0^2(\eta)} \quad (3)$$

where k_B is Boltzmann's constant, e is the charge of single electron, F_n are Femi integrals of order n and η is reduced Fermi energy. The last quantity can be determined from the Seebeck coefficient data using[29]

$$S = \pm\frac{k_B}{e}\left(2\frac{F_1(\eta)}{F_0(\eta)} - \eta\right) \quad (4)$$

The lattice thermal conductivity of $Cu_{12}Sb_4S_{13-x}Se_x$ (x = 0, 0.5, 1), displayed in Figure 4 (center), decreases with increasing temperature, which is typical for most of TE materials at high temperatures where phonon-phonon scattering dominates. The lattice thermal conductivity is reduced from 0.61 W/m K to 0.33 W/m K at 720 K, a value approaching the amorphous limit[30] for tetrahedrite. While the lattice thermal conductivity of all tetrahedrites is low, due to the strong anharmonicity of the lattice vibrational spectrum[31-33], Se substitution induces additional scattering of phonons due to the large mass difference between S and Se atoms. The resulting reduction in lattice thermal conductivity compensates for the increase in the electronic portion, further lowering the total thermal conductivity. Thus, Se substitution also successfully decouples the electrical resistivity and total thermal conductivity in tetrahedrite.

The combination of increased power factor and reduced total thermal conductivity results in an enhancement of the dimensionless figure of merit, Figure 4 (lower), in $Cu_{12}Sb_4S_{13-x}Se_x$ (x = 0.5, 1, 2). The x = 1 sample has the maximum ZT value of 0.86 at 720 K, a nearly 40 % increase over that of $Cu_{12}Sb_4S_{13}$. This value is comparable to that reported for transition metal substituted tetrahedrite, but in this case the increase occurs through enhancement of the power factor.

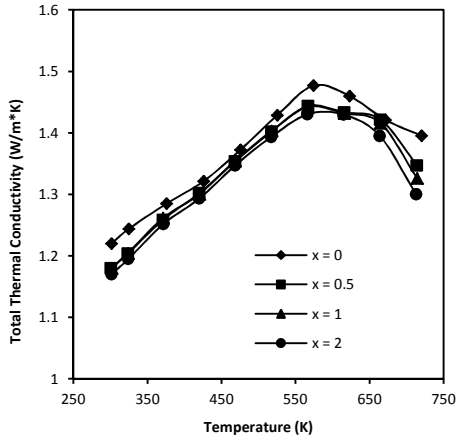

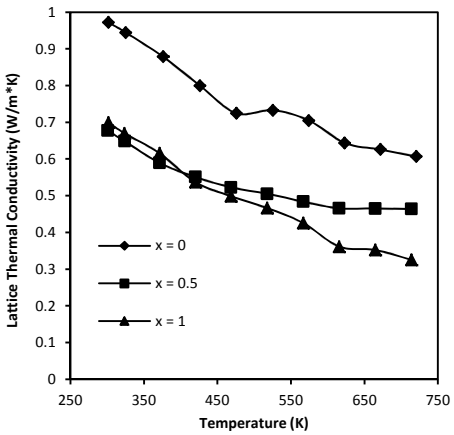

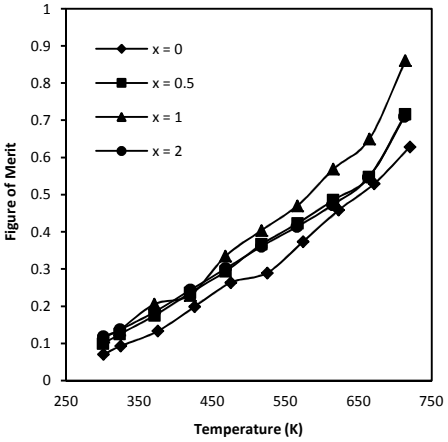

Figure 4. Temperature dependence of the total thermal conductivity, lattice thermal conductivity and figure of merit of $Cu_{12}Sb4S1_{3-x}Se_x$ (x = 0, 0.5, 1, 2). The total thermal conductivity (upper) is decreased at high temperature with Se, addition due to a strong decrease in lattice thermal conductivity (center). This, combined with the increased power factor, results in an enhanced thermoelectric figure of merit in Se-substituted samples.

CONCLUSION

In summary, we present a new path for enhancing figure of merit by decoupling the Seebeck coefficient, electrical resistivity and total thermal conductivity in tetrahedrite through Se substitution. We show that, due to band degeneracy and convergence effects, with Se substitution the electrical resistivity is decreased without diminution of the Seebeck coefficient, leading to an enhanced thermoelectric power factor and thermoelectric figure of merit. Based on these results, it is speculated that further improvement in figure of merit of tetrahedrite can be achieved by co-doping with transition metal elements and Se. These materials are earth-abundant, cost-effective alternatives to traditional thermoelectric materials and may lead to very widespread usage for power generation from waste heat sources.

Associated Content

Supporting Information

The Supporting information is available free of charge on the ACS Publications website at

Two figures, displaying lattice constant as a function of Se content and Rietveld analyses of the synchrotron XRD and lab XRD of $Cu_{12}Sb_4S_{12}Se$ at room temperature. Two tables, showing detailed synchrotron XRD crystallographic structure analysis results of $Cu_{12}Sb_4S_{12}Se$ based on single phase and two phase model.

AUTHOR INFORMATION

Corresponding Author

*(X. L.) *; (D.T.M.) email:
luxu@cqu.edu.cn; dmorelli@egr.msu.edu

Author Contributions

The manuscript was written through contributions of all authors. All authors have given approval to the final version of the manuscript.

ACKNOWLEDGMENT

This work This work was supported as part of the Center for Revolutionary Materials for Solid State Energy Conversion, an Energy Frontier Research Center funded by the U.S. Department of Energy, Office of Science, Office of Basic Energy Sciences under Award Number DE-SC0001054. X. L. also acknowledged the financial support from the Fundamental Research Funds for the Central Universities of China (Project No. 0903005203360). We used computing resources at the National Energy Research Scientific Computing Center, which is supported by the US DOE under Contract No. DE-AC02-05CH11231. Use of the Advanced Photon Source at Argonne National Laboratory was supported by the U. S. Department of Energy, Office of Science, Office of Basic Energy Sciences, under Contract No. DE-AC02-06CH11357.

REFERENCES

(1) Slack, G.A. *CRC Handbook of Thermoelectrics*, ed. D.M. Rowe, CRC Press, Boca Raton, FL 1995.

(2) Lu, X.; Morelli, D.T.; Xia, Y.; Zhou, F.; Ozolins, V.; Chi, H.; Zhou, X.; Uher, C. High Performance Thermoelectricity in Earth-AbundantCompounds Based on Natural Mineral Tetrahedrites. *Adv. Energy Mater.* **2012**, *3*, 342-348.

(3) Lu, X.; Morelli, D.T. Natural Mineral Tetrahedrite as a Direct Source of Thermoelectric Materials *Phys. Chem. Chem. Phys.* **2013**, *15*, 5762-5766.

(4) Lu, X.; Morelli, D.T. Rapid Synthesis of High-Performance Thermoelectric Materials Directly from Natural Mineral Tetrahedrite. *MRS Commun*. **2013**, *3*, 129-133.

(5) Suekuni, K.; Tsuruta, K.; Ariga, T.; Koyano, M. Thermoelectric Properties of Mineral Tetrahedrites $Cu_{10}Tr_2Sb_4S_{13}$ with Low Thermal Conductivity. *Appl. Phys. Express* **2012**, *5*, 051201.

(6) Suekuni, K.; Tsuruta, K.; Kunii, M.; Nishiate, H.; Nishibori, E.; Maki, S.; Ohta, M.; Yamamoto, A.; Koyano,

M. High-Performance Thermoelectric Mineral $Cu_{12-x}Ni_x Sb_4S_{13}$Tetrahedrite. *J. Appl. Phys.* **2013**, *113,*043712.

(7) Heo, J.; Laurita, G.; Muir, S.; Subramanian, M.A.; Keszler, D.A. Enhanced Thermoelectric Performance of Synthetic Tetrahedrites. *Chem. Mater.* **2014**, *26*, 2047-2051.

(8) Barbier, T.; Lemoine, P.; Gascoin, S.; Lebedev, O. I.; Kaltzoglou, A.; Vaqueiro, P.; Powell, A. V.; Smith, R. I.; Gulimeau, E. Structural Stability of the Synthetic Thermoelectric Ternary and Nickel-Substituted Tetrahedrite Phases. *J. Alloys Compd.* **2015**, *634*, 253-262.

(9) Chetty, R.; Bali, A.; Naik. M. H.; Rogl, G.; Rogl, P.; Jain, M.; Suwas, S.; Mallik, R. C. Thermoelectric Properties of Co Substituted Synthetic Tetrahedrite. *Acta Mater.* **2015**, *100*, 266-274.

(10) Lu, X.; Morelli, D. T.; Xia, Y.; Ozolins, V. Increasing the Thermoelectric Figure of Merit of Tetrahedrites by Co-doping with Nickel and Zinc. *Chem. Mater.* **2015**, *27*, 408-413.

(11) Lu, X.; Morelli, D. T. The Effect of Te Substitution for Sb on Thermoelectric Properties of Tetrahedrite. *J. Electron. Mater.* **2013**, *43*, 1983-1987.

(12) Bouyrie, Y.; Candolfi, C.; Ohorodniichuk, V.; Malaman, B.; Dauscher, A.; Tobolab, J.; Lenoir, B. Crystal Structure, Electronic Band Structure and High-Temperature Thermoelectric Properties of Te-Substituted Tetrahedrites $Cu_{12}Sb_{4-x}Te_xS_{13}$ ($0.5 \leq x \leq 2.0$). *J. Mater. Chem. C* **2015**, *3*, 10476-10487.

(13) Zhang, Y.; Ozoliņš, V.; Morelli, D.T.; Wolverton, C. Prediction of New Stable Compounds and Promising Thermoelectrics in the Cu–Sb–Se System. *Chem. Mater.* **2014**, *26* 3427-3435.

(14) Kresse, G.; Hafner, J. Ab initio Molecular Dynamics for Liquid Metals. *Phys. Rev. B* **1993**, *47*, 558-561.

(15) Kresse, G.; Hafner, J. Ab initio Molecular-Dynamics Simulation of the Liquid-Metal–Amorphous-Semiconductor Transition in Germanium. *Phys. Rev. B***1994**, *49***,** 14251-14269.

(16) Kresse, G.; Furthmüller, J. Efficient Iterative Schemes for Ab initio Total-Energy Calculations Using a Plane-Wave Basis Set. *Phys. Rev. B* **1996,** *54***,** 11169-11185.

(17) Kresse, G.; Furthmüller, J. Efficiency of Ab-initio Total Energy Calculations for Metals and Semiconductors Using a Plane-Wave Basis Set. *Comput. Mater. Sci.* **1996,** *6***,** 15-50.

(18) Perdew, J.P.; Burke, K.; Ernzerhof, M. Generalized Gradient Approximation Made Simple. *Phys. Rev. Lett.* **1996,** *77,* 3865-3868.

(19) Perdew, J.P; Burke, K.; Ernzerhof, M. Generalized Gradient Approximation Made Simple. *Phys. Rev. Lett.* **1997,** *78,* 1396.

(20) Akbarzadeh, A.R.; Ozoliņš, V; Wolverton, C. First-Principles Determination of Multicomponent Hydride Phase Diagrams: Applications to the Li-Mg-N-H System. *Adv. Mater.* **2007**, 19, 3233-3239.

(21) Petricek, V.; Dusek, M.; Palatinus, L. Z. Crystallographic Computing System JANA2006: General Features. *Z. Kristallogr.* **2014**, *229*, 345-352.

(22) Wuensch, B. J. The Crystal Structure of Tetrahedrite, $Cu_{12}Sb_4S_{13}$. *Z. Kristallogr.* **1964**, *119*, 437-453.

(23) Pfitzner, A.; Evain, M.; Petricek, V. $Cu_{12}Sb_4S_{13}$: A Temperature-Dependent Structure Investigation. *ActaCryst.* **1997**, B53, 337-345.

(24) Lai, W.; Wang, Y.; Morelli, D. T.; Lu, X. Thermoelectrics: From Bonding Asymmetry to Anharmonic Rattling in $Cu_{12}Sb_4S_{13}$Tetrahedrites: When Lone Pair Electrons Are Not So Lonely. *Adv. Funct. Mater.* **2015**, *25*, 3648-3657.

(25) Bouyrie, Y.; Candolfi, C.; Dauscher, A.; Malaman, B.; Lenoir, B. Exsolution Process as a Route toward Extremely Low Thermal Conductivity in $Cu_{12}Sb_{4-x}Te_xS_{13}$ Tetrahedrites. *Chem. Mater.* **2015**, 27, 8354−8361.

(26) Lu, X.; Morelli, D.T.; Zhang, Y.; Wolverton, C. Thermoelectric Power Factor Enhancement in Tetrahedrites. APS March Meeting **2014**: http://meetings.aps.org/link/BAPS.2014.MAR.L25.2

(27) Pei, Y.; Shi, X.; LaLonde, A.; Wang, H.; Chen, L.D.; Snyder, G.J. Convergence of Electronic Bands for High Performance Bulk Thermoelectrics. *Nature* **2011**, *473*, 66-69.

(28) Liu, W.; Tan, X.; Yin, K.; Liu, H.; Tang, X.; Shi, J.; Zhang Q.; Uher, C. Convergence of Conduction Bands as a Means of Enhancing Thermoelectric Performance of N-Type $Mg_2Si_{1-x}Sn_x$ Solid Solutions. *Phys. Rev. Lett.* **2012**, 108, 166601.

(29) Fistul, V.I. *Heavily Doped Semiconductors*; Plenum: New York, 1969.

(30) Cahill, D.G.; Pohl, R.O. Thermal Conductivity of Amorphous Solids above the Plateau. *Phys. Rev. B* **1987**, *35*, 4067-4073.

(31) Lara-Curzio, E.; May, A. F.; Delaire, O., McGuire, M. A.; Lu, X.; Liu, C.; Case, E. D.; Morelli, D. T. Low-Temperature Heat Capacity and Localized Vibrational Modes in Natural and Synthetic Tetrahedrites. *J. Appl. Phys.* **2014**, *115*, 193515.

(32) Bouyrie, Y.; Candolfi, C.; Pailhes, S.; Koza, M. M.; Malaman, B.; Dauscher, A.; Tobolab, J.; Boisron, O.; Saviot, L.; Lenoir, B. From Crystal to Glass-Like Thermal Conductivity in Crystalline Minerals. *Phys. Chem.Chem. Phys.* **2015**, *17*, 19751-19758.

(33) Zhou, F.; Nielson, W.; Xia, Y.; Ozolins, V. Lattice Anharmonicity and Thermal Conductivity from Compressive Sensing of First-Principles Calculations. *Phys. Rev. Lett.* **2014**, *113*, 185501.
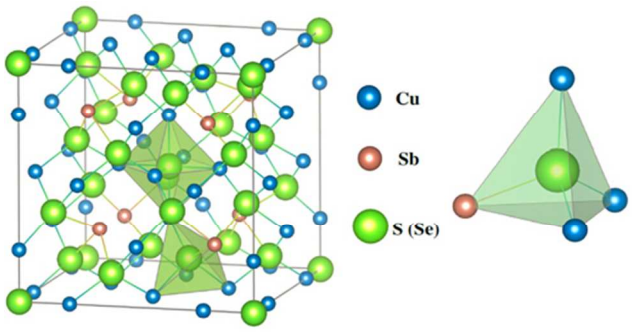
Table of Contents Figure: